



OPEN Computational discovery of novel aryl hydrocarbon receptor modulators for psoriasis therapy

Gianluca Santini¹, Laura Bonati¹✉ & Stefano Motta^{1,2}✉

The aryl hydrocarbon receptor (AhR) is a ligand-dependent transcription factor involved in the regulation of many pathophysiological processes. Among these, immune system modulation, as well as regulation of skin homeostasis and inflammation, make it a promising target for psoriasis therapy. Tapinarof, an AhR agonist recently approved for psoriasis treatment, exerts its action through antioxidant, anti-inflammatory and barrier-restoring effects. In this study, we employed a computational drug-discovery approach to identify novel AhR modulators with psoriasis therapeutic potential. We performed a multi-step similarity-based screening in PubChem. Molecular docking led to the identification of diverse chemical scaffolds with high docking scores and potential AhR activity, some belonging to chemical classes with known pharmacological relevance. The stability of the binding geometries of the most promising compounds of each family was then verified through molecular dynamics simulations and pharmacokinetic characteristics were predicted using ADMETlab 2.0 and SwissADME. Notably, several identified compounds suggest a possible interplay between AhR signaling and sirtuin modulation, highlighting a previously unexplored avenue in psoriasis therapy. Our findings underscore the potential of computational approaches in accelerating the discovery of novel AhR-targeting agents and provide a foundation for further experimental validation.

The aryl hydrocarbon receptor (AhR) is a ligand-dependent transcription factor that plays a pivotal role in mediating various cellular and metabolic responses^{1–3}. Binding to and activation of the AhR by a diverse array of exogenous and endogenous compounds leads to the induction or inhibition of diverse gene expression pathways and the production of a broad spectrum of toxic and biological effects, including cell growth, differentiation, apoptosis, and immune system modulation^{4–8}. Initially believed to be activated only by planar, hydrophobic molecules, such as the widely studied halogenated aromatic hydrocarbons (HAHs), which can elicit toxic effects⁹, AhR is now recognized as a receptor for a diverse range of environmental and endogenous ligands^{10–12}. The effects of AhR activation may depend on the type of ligand, its concentration, and the specific binding site involved. An example of this complexity is the opposing effects induced on CD4⁺ T cell differentiation by the high-affinity agonists FICZ and TCDD^{13,14}. Moreover, significant overlap between AhR ligands and those of other promiscuous receptors, such as PXR, suggests that crosstalk with other transcription factors may contribute to ligand-specific responses^{15,16}.

AhR may exert its function through either canonical or non-canonical signaling pathways^{4,6}. The canonical AhR signaling pathway involves ligand binding to the PAS-B domain of AhR in the cytosol, where it is complexed with the chaperone heat shock protein 90 (hsp90), the co-chaperone XAP2, and the p23 protein. hsp90 protects AhR from degradation, retains the complex within the cytoplasm, and maintains AhR in an inactive state by masking its nuclear localization sequence (NLS). Upon ligand binding, the AhR:hsp90 complex undergoes a conformational change that facilitates its translocation into the nucleus and conversion into its high-affinity DNA-binding form¹⁷. During this process, AhR dissociates from the chaperone proteins and dimerizes with the homologous AhR nuclear translocator (ARNT). Finally, the ligand:AhR:ARNT complex binds to a specific DNA recognition site, the dioxin-responsive element (DRE), leading to gene transcription¹⁸. The non-canonical functions of AhR are diverse, context-dependent, and often tissue- or ligand-specific. AhR has been found to interact with various key cellular signaling pathways that are critical for normal physiological processes, as well as in the pathogenesis of several diseases^{1,2,6}. For this reason, the development of new therapeutic molecules targeting AhR is becoming increasingly promising. However, the lack of experimentally determined atomic structures of the AhR ligand-binding domain has hindered accurate in-silico predictions for a long time. The recent determination of the cryo-EM structure of the AhR:hsp90:XAP2:p23 cytosolic complex marked a

¹Department of Earth and Environmental Sciences, University of Milano-Bicocca, Milan 20126, Italy. ²Inter-University Center for the Promotion of the 3Rs Principles in Teaching & Research (Centro 3R), Pisa 56122, Italy. ✉email: laura.bonati@unimib.it; stefano.motta@unimib.it

significant advancement¹⁹, enabling the use of an experimental structure as a model for in-silico investigations of AhR-ligand binding rather than relying solely on homology models^{20–24}. Furthermore, the subsequent release of experimental AhR structures in different bound and unbound forms^{25,26} has provided insights into ligand-induced conformational changes within the ligand-binding cavity. Notably, while we had already completed our computational analysis, a set of X-ray structures of the AhR:ARNT dimer complexed with some of the most studied AhR ligands (tapinarof, indirubin, FICZ, benzo[a]pyrene (BaP), β -Naphthoflavone, and indigo) became available²⁷. These newly resolved structures further illustrate how different ligands stabilize distinct conformations of the receptor, reinforcing our understanding of ligand-induced adaptations. Such insights enhance the accuracy of in-silico modeling of AhR-ligand interactions, paving the way for more reliable computational screening approaches to identify novel AhR modulators with potential therapeutic applications.

Among the potential therapeutic applications of AhR ligands, one found clinical application in May 2022, when the U.S. FDA approved a cream containing 1% of the AhR agonist tapinarof for the topical treatment of plaque psoriasis in adults²⁸. Tapinarof is a naturally-derived hydroxylated stilbene (stilbenoid) produced by bacterial symbionts of entomopathogenic nematodes. Stilbenoids, such as resveratrol, are well-known for their diverse biological activities, including anti-inflammatory²⁹, anti-proliferative³⁰, and anti-cancer³¹ effects, many of which are mediated through interactions with multiple cellular targets, including nuclear factor kappa B (NF- κ B)³², sirtuins³³ and AhR³⁴. The ability of resveratrol and its derivatives to modulate AhR activity, sometimes with contrasting effects, highlights the complexity of AhR-ligand interactions and their therapeutic potential^{34–39}. Following the discovery of the therapeutic effects of tapinarof cream in psoriasis patients^{40–42}, Smith et al. identified AhR as the primary target through which tapinarof exerts its efficacy in inflammatory skin conditions⁴³. Tapinarof acts through multiple mechanisms, including immune regulation, skin barrier restoration, and oxidative stress reduction⁴⁴. By activating AhR, tapinarof suppresses Th17/Th22-driven inflammation, downregulating key cytokines such as IL-17 A, IL-17 F, and IL-22, which are central to psoriasis pathogenesis⁴³. Additionally, tapinarof promotes keratinocyte differentiation and enhances skin barrier integrity by upregulating essential structural proteins such as filaggrin and loricrin⁴³. Its antioxidant properties, mediated through both direct ROS scavenging and AhR-Nrf2 pathway activation⁴⁵, further contribute to its therapeutic efficacy. However, the fact that the effects of tapinarof are solely due to AhR activation has been debated, suggesting that additional AhR-independent mechanisms might also contribute to its therapeutic action⁴⁶.

The aim of this work was to identify molecular scaffolds with the potential to bind and activate AhR and to exert therapeutic effects against psoriasis-related inflammation by employing computational approaches. To achieve this, we first used molecular docking to predict the binding mode of tapinarof in the human AhR PAS-B domain, identifying key interactions that stabilize its pose. Based on these insights, we implemented a multistage search strategy to systematically explore the chemical space in PubChem. To explore a broad range of potential AhR ligands, we used diverse similarity-based strategies implemented in PubChem, leading to an initial library of 19,943 compounds. The screening of these compounds by docking identified four promising chemical families with consistently high docking scores and a substructure-based expansion of these allowed us to retrieve additional 77,359 molecules from PubChem. The docking results on the final set of compounds highlighted several families with optimal docking profiles and intriguing characteristics. While some exhibited structural similarity to tapinarof, differing only in minor modifications to the stilbene scaffold, others displayed significant distinctive features. To verify the stability of the docking poses of the most promising compounds of each family, molecular dynamics (MD) simulations of the complexes were performed, revealing that most of them are as stable as tapinarof. Finally, we also performed ADMET investigation to assess the pharmacokinetic characteristics of the selected compounds. Interestingly, a review of the relevant literature revealed that some of these compounds are implicated in biological pathways associated with psoriasis, underscoring their relevance and warranting further investigation as potential novel AhR modulators.

Results

Tapinarof binding mode predicted by Docking

To understand the molecular interactions between tapinarof and AhR, we first performed docking calculations to predict its binding mode. Our docking analysis was based on the experimental structure of the human AhR PAS-B domain in complex with indirubin (PDB ID 7ZUB)¹⁹, ensuring a well-represented ligand-binding site. Tapinarof, an AhR agonist, exhibits a binding affinity of 100–200 nM toward the AhR ligand-binding domain⁴³. The docking score obtained for tapinarof was -10.6 kcal/mol, consistent with the redocking score of indirubin (-11.3 kcal/mol), which is expected to have a higher affinity. The predicted binding mode revealed key interactions between tapinarof and critical residues in the receptor binding cavity (Fig. 1).

These interactions include hydrogen bonds with the side chain of Gln383 and the backbone carbonyl of Gly321, as well as aromatic π -stacking with Phe295 and His291. The predicted pose aligns well with the binding mode observed in the recently available porcine AhR X-ray structure bound to tapinarof²⁷ (PDB ID: 8XS6), with an RMSD of 0.6 Å between the two (Supplementary Fig. 1). Moreover, the interactions established by tapinarof are the same found for other AhR ligands, such as indirubin (Supplementary Fig. 2) and BaP^{19,25}. Among these, the most stabilizing interaction was with Phe295, which appears to play a key role in defining the ligand orientation within the binding site. Specifically, Phe295 dictates the plane in which the ligand lies, as its aromatic side chain provides a crucial π -stacking surface. Given that most AhR ligands possess planar aromatic scaffolds, it is conceivable that they align parallel to the Phe295 side chain to establish a strong π - π interaction, which likely contributes to their binding affinity.

Docking of PubChem molecules identified by 3D similarity to tapinarof

To explore structurally-related compounds with potential AhR activity, we performed a 3D similarity search in PubChem using tapinarof as the query (Supplementary Fig. 3). This approach identified a set of 305 candidate

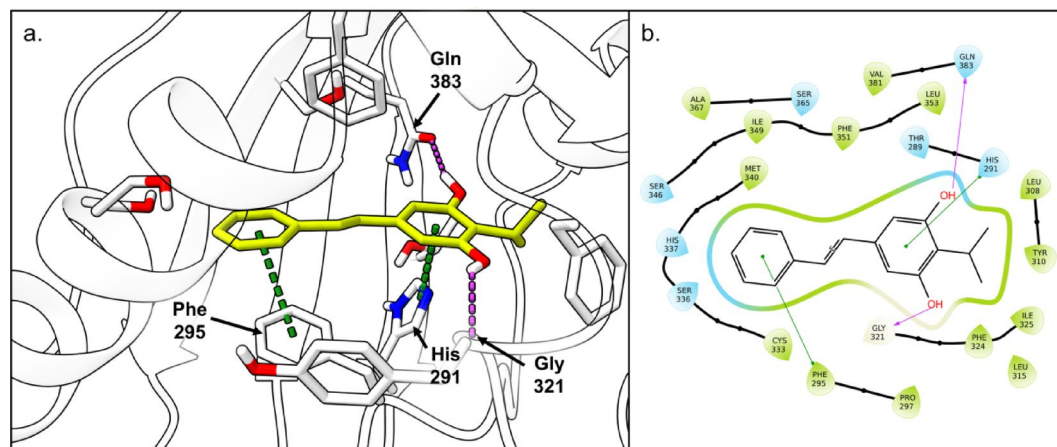


Fig. 1. Binding mode of tapinarof within the AhR PAS-B domain. **(a)** 3D representation of the binding pose: tapinarof is depicted in yellow sticks; protein is shown as white cartoon; relevant residues are represented in white sticks; π -stacking interactions are shown with green dashed lines; H-bonds are represented as magenta dashed lines. **(b)** 2D representation of the tapinarof interactions.

molecules sharing similar molecular shape and pharmacophoric features with tapinarof. Each of these compounds was then docked into the AhR ligand-binding domain to assess their potential binding affinity and interaction patterns. Of these 305 candidates, 90 compounds exhibited docking scores comparable to or better than that of tapinarof. Analysis of these compounds revealed that most exhibit only minor modifications relative to tapinarof (hereafter referred to as “tapinarof close analogues”). These modifications primarily include: hydroxylation at one or multiple positions on one or both aromatic rings; fluorination at one or multiple positions at one or both aromatic rings; and substitution of the isopropyl group with cyclopentane or cyclohexane (Supplementary Fig. 4). The binding mode of these molecules closely resembles that of tapinarof (Fig. 2a), with additional hydroxyl groups capable of forming hydrogen bonds with residues within the binding cavity. Specifically, we observed that Ser336 and Ser346 were commonly predicted to establish hydrogen bonds with these hydroxyl groups.

In addition to these tapinarof close analogues, we identified three other subfamilies of compounds that consistently exhibited favorable docking scores.

- **Condensed Rings** (Fig. 2b): This family comprises molecules in which the central double bond of the stilbene scaffold undergoes cyclization, forming a fused ring system. These rings range from simple naphthalene-like structures to five- or six-membered nitrogen- or oxygen-containing heterocycles, always forming at the unsubstituted ring of tapinarof (Supplementary Fig. 5). This cyclization enhances π -stacking interactions with Phe295, while the hydroxylated ring maintains the characteristic hydrogen bonds with the side chain of Gln383 and the backbone carbonyl of Gly321.
- **Benzyl Addition on Central Linker** (Fig. 2c): This family includes a small number of molecules featuring a benzyl group attached to the central double bond of tapinarof (Supplementary Fig. 6). Notably, this additional ring forms an extra π -stacking interaction with Tyr322, which may contribute to increased binding stability.
- **Aryl Addition to Isopropyl** (Fig. 2d): Compounds in this family feature an aryl ring replacing one of the methyl groups of the isopropyl moiety of tapinarof (Supplementary Fig. 7). This substitution significantly increases the molecular length, making it incompatible with the original tapinarof binding mode. Additionally, the added aryl ring exhibits considerable conformational flexibility, an uncommon characteristic among high-affinity AhR ligands. For these reasons, this family appears less promising compared to the others.

All these compounds maintain a high degree of similarity to tapinarof and remain structurally very close to the original molecule. Therefore, most of them are covered by existing tapinarof patents. This limitation prompted us to expand our search beyond these close analogs, exploring alternative scaffolds that could retain strong AhR binding potential while introducing more significant structural diversity.

Docking of tapinarof analogues: expanding the dataset with structural variants

To explore a broader range of potential AhR ligands, we expanded our search in PubChem using alternative similarity-based strategies beyond the initial 3D similarity approach (see Methods section). This allowed us to construct a second, more diverse library comprising 19,943 compounds. The goal of this step (summarized in Supplementary Fig. 8) was to introduce greater structural variability while preserving key pharmacophoric features essential for AhR binding. Each of the compounds in the library retrieved by PubChem was subjected to docking calculations, leading to the identification of four promising chemical families characterized by consistently high docking scores: (i) tolans, analogues of stilbenoids but with triple bonds instead of the central double bond; (ii) alkene to three-membered ring cyclization, in which the central double bond is substituted by a cyclopropyl, epoxide, or aziridine moiety; (iii) phenyl benzoate derivatives, featuring an ester-linked biphenyl system; (iv) alkene to imine/azo, where the central double bond is replaced by a C = N or N = N linkage.

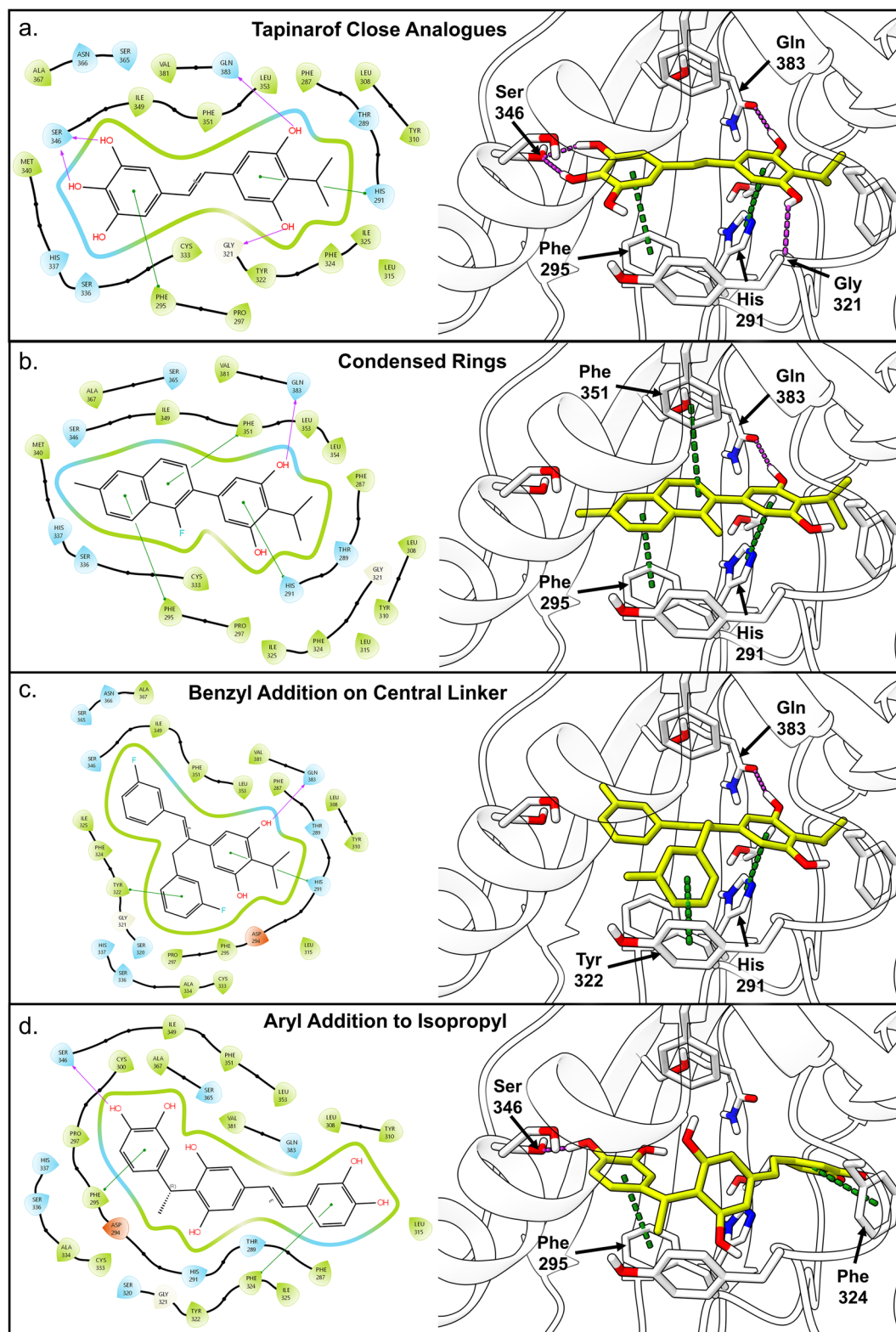


Fig. 2. Binding modes of the most promising scaffolds identified through a 3D similarity search using tapinarof as the query molecule. For each family, the compound with the best docking score is shown. (a) tapinarof close analogues; (b) condensed rings; (c) benzyl addition on central linker; (d) aryl addition to isopropyl. 2D representation of the ligand interactions are shown in the left panels, while 3D representations of the binding pose are shown in the right panels.

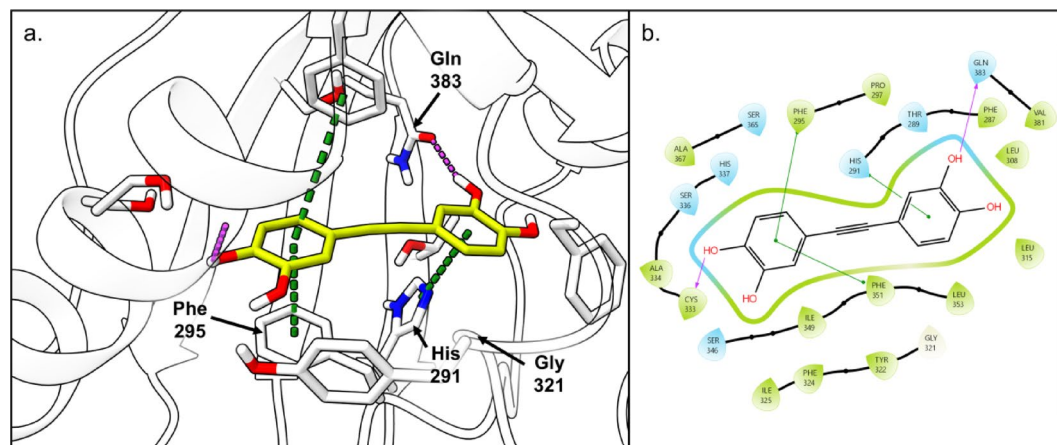


Fig. 3. Binding mode of the compound with the best docking score belonging to the tolan family. **(a)** 3D representation of the binding pose: ligand is depicted in yellow sticks; protein is shown as white cartoon; relevant residues are represented in white sticks; π -stacking interactions are shown with green dashed lines; H-bonds are represented as magenta dashed lines. **(b)** 2D representation of the ligand interactions.

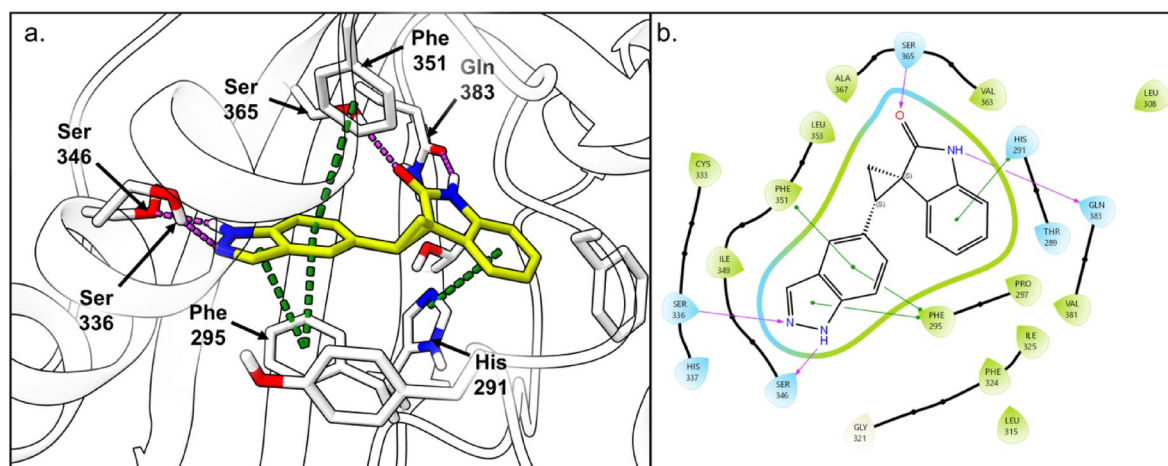


Fig. 4. Binding mode of the compound with the best docking score belonging to the “alkene to three-membered ring cyclization” family. **(a)** 3D representation of the binding pose: ligand is depicted in yellow sticks; protein is shown as white cartoon; relevant residues are represented in white sticks; π -stacking interactions are shown with green dashed lines; H-bonds are represented as magenta dashed lines. **(b)** 2D representation of the ligand interactions.

Since these families were particularly promising due to their divergence from compounds already described in the tapinarof patents, we refined our exploration within these newly identified chemical families. To achieve this, we performed a substructure-based expansion using the minimal scaffold representing each family, retrieving an additional 77,359 compounds from PubChem. This approach allowed us to systematically investigate structural variations within the most promising scaffolds and identify compounds that exhibited optimal interaction patterns. In the following section, the properties, binding modes, and interactions of the most promising compounds from the different chemical families are discussed.

- Tolans:** This family consists of two phenyl groups attached to both ends of a $-C \equiv C-$ (ethynyl) linker. These molecules are closely related to stilbenes as it is possible to obtain a stilbene by simple partial hydrogenation of the central triple bond. The most promising compounds here identified are hydroxylated tolans in which at least one of the two phenyl groups is substituted with at least one -OH group. The compound with the best score (-12.45 kcal/mol) identified within this family is shown in Fig. 3. It contains four hydroxyl groups, two on each ring. Interestingly, the positioning of these groups does not allow for the preservation of the hydrogen bond with Gly321. At the opposite end of the molecule, the hydroxyl group in the para position forms a hydrogen bond with the backbone carbonyl of Cys333. Supplementary Fig. 9a-c shows additional compounds belonging to the tolan family. These comprise compounds hydroxylated at different positions and molecules that feature various substituents at one of the rings or condensed rings on one side.

- **Phenyl benzoate derivatives:** This family of compounds was originally included among the most promising compounds, as we noted that the substitution of the stilbenes central double bond with an ester group could be a promising modification. However, after refinement of the search through the substructure function, we surprisingly discovered a high number of molecules with docking scores significantly lower than the one obtained for tapinarof, but in which the ester group forms an additional condensed cycle (lactonization). Thus, the resulting molecules present three or more condensed aromatic rings. The compound with the highest docking score (-12.95 kcal/mol) presents four condensed rings that establish an extensive π -stacking network with residues Phe295 and Phe351 (Fig. 5). Moreover, H-bonds with Ser346, Ser336 and Gly321 anchor the molecule at opposite sides. Supplementary Fig. 12a-c shows additional compounds belonging to this family.
- **Alkene to imine/azo:** This family of compounds yielded the largest dataset of ligands, with 58,445 compounds retrieved from PubChem. The substitution of one or both carbon atoms in the central double bond of stilbenes (as in *N*-benzylideneaniline and azobenzene, respectively) provides a flexible scaffold, where the central linker can accommodate an additional fused ring (a feature frequently observed in the phenyl benzoate family as well). Many compounds of this family share a 2-hydroxyquinoxaline ring, with the best compound showing a docking score of -13.84 kcal/mol. This recurrent motif forms H-bonds with Gln383 and Ser365 and engages in π -stacking with His291 (Fig. 6). The second ring is stabilized by π -stacking interactions with Phe295 and Phe351. Overall, the two aromatic systems lie almost in the same plane, with an interplanar angle of approximately 20° . Additional compounds from this family are shown in Supplementary Fig. 13a-c.

Assessment of stability through molecular dynamics simulations

Incorporating MD simulations into docking studies is essential to account for the dynamic behavior of protein-ligand complexes, allowing for a more accurate refinement of binding poses by explicitly considering receptor flexibility and conformational adaptability⁴⁸. To assess the stability and the dynamic behavior of the predicted ligand-protein complexes, MD simulations were performed for tapinarof and the four most representative compounds from each of the identified chemical families. For each complex, three independent 100 ns simulations were conducted, resulting in a comprehensive evaluation of ligand binding stability. The root-mean-square deviation (RMSD) of the ligand was analyzed to quantify the stability of ligand-protein interactions over time (Supplementary Fig. 14). Both tapinarof and the tolan compounds exhibited remarkable stability throughout the simulations, with ligand RMSD consistently below 2 Å, suggesting a well-maintained binding mode. In contrast, some of the compounds in the “Alkene to three-membered ring cyclization” and “Phenyl benzoate derivatives” families displayed significantly higher RMSD values across all replicates. Specifically, the fourth compound of the former and the first and second compounds of the latter one exhibited consistently elevated RMSD, indicating reduced binding stability and a tendency to adopt alternative conformations within the binding site. Conversely, the “Alkene to imine/azo” family displayed a high degree of stability across all tested compounds, suggesting a favorable binding profile for this class of molecules.

To further investigate the binding affinity of the studied compounds, molecular mechanics/generalized Born surface area (MMGBSA) calculations were performed to estimate the binding free energy over the course of the simulations. The results of these analyses are shown in Supplementary Fig. 15, where the computed binding free energies exhibit fluctuations around a well-defined mean value in all simulations. Tapinarof exhibited a mean binding free energy of approximately -36 kcal/mol, consistent with its known high-affinity for AhR. Notably, compounds that displayed higher RMSD values, indicative of lower binding stability, also displayed less favorable MMGBSA energy estimates, with values less negative than -30 kcal/mol. This trend was particularly evident for the least stable compounds from the “Alkene to three-membered ring cyclization” and “Phenyl benzoate derivatives” families. Interestingly, the first tolan derivative and the third compound of the “Alkene to imine/azo” family exhibited slightly less negative binding free energies compared to their respective family members, suggesting potential differences in the affinity of these ligands.

In silico pharmacokinetics and toxicity assessment

Pharmacokinetics analysis is crucial for understanding how a compound interacts with the human body, influencing both its therapeutic effects and adverse outcomes. In this study, we employed ADMETlab 2.0⁴⁹ to evaluate the pharmacokinetic properties of our most promising compounds, analyzing 88 characteristics across seven categories. Additionally, SwissADME⁵⁰ was used to calculate the skin permeation parameter (log Kp). The tapinarof profile was also computed using these tools for comparison with our representative compounds. The reference compounds (comp. 1) for each family adhere to Lipinski's Rule of Five⁵¹, the GSK Rule⁵², and the Golden Triangle⁵³, suggesting a favorable ADMET profile. The primary physicochemical properties, including molecular weight, volume, logP, and others, are summarized in Supplementary Table 1.

The tolan molecule with the best docking score (Tolans comp. 1), contains four hydroxyl groups, making it more hydrophilic than tapinarof. This increased hydrophilicity may reduce its skin permeability, although for topical drugs limited permeation could be advantageous, potentially minimizing systemic absorption and side effects. Regarding the “Phenyl benzoate derivatives” and “Alkene to imine/azo” families, the reference compounds exhibited higher logP values and increased skin permeability (log Kp). The reference compound in the “Alkene to three-membered ring cyclization” family displayed a very low log Kp, though other members of this family showed better permeability properties. The Total Polar Surface Area (TPSA) was also assessed as an estimate of skin permeability. While the reference compounds from all four families had a larger TPSA than tapinarof, the values remained below 91 \AA^2 , indicating that skin permeation is still feasible.

Additional absorption parameters were calculated, and all reference compounds exhibited acceptable values, with no concerning results.

For distribution, we observed a high tendency to plasma protein binding (> 90%) for the reference compounds, which is not problematic for topical drugs. The volume of distribution (Vd) parameters indicated a favorable balance between plasma and tissue partitioning. The top compounds in the “Alkene to imine/azo” and “Alkene to three-membered ring cyclization” group showed a higher likelihood of crossing the blood-brain barrier; however, other members of these families presented safer profiles. Again, this aspect is not overly problematic for topical drugs, which usually present lower systemic distributions.

Metabolic evaluation focused on the inhibition potential of five key cytochrome P450 isozymes (CYP1A2, CYP2C19, CYP2C9, CYP2D6, and CYP3A4), responsible for approximately 80% of drug metabolism. Inhibition of these isozymes could increase the risk of drug-drug interactions and bioaccumulation. Interestingly, the “Tolans” and “Alkene to imine/azo” reference compounds exhibited lower predicted inhibitory activities for all five isozymes compared to tapinarof. Regarding excretion, the clearance rates for the reference compounds were moderate to high (> 5 ml/min/kg).

Toxicological assessment is an essential part of drug development to evaluate safety for human use. Carcinogenicity predictions revealed concerns for the “Tolans”, “Alkene to three-membered ring cyclization”, and “Phenyl benzoate derivatives” families. Specifically, the first two families showed a higher probability in the Carcinogenicity parameter, which correlates well with the prediction of being Ames-positive, suggesting mutagenic potential. The best compound in the “Phenyl benzoate derivatives” family, although showing lower carcinogenicity risk, contains a condensed polycyclic aromatic scaffold, which is flagged as a potential toxicophore. Notably, the member of the “Tolans” family shown in Supplementary Fig. 9c (“Tolans” comp. 4) has acceptable carcinogenicity and Ames test values, without mutagenic toxicophore alerts. This molecule mirrors tapinarof, but with a triple bond between the aromatic rings. In the “Phenyl benzoate derivatives” family, the compound in Supplementary Fig. 12b (Phenyl benzoate derivatives comp. 3) does not feature a polycyclic aromatic scaffold, reflecting a safer profile. None of the reference compounds showed predicted cardiotoxicity. However, the “Alkene to imine/azo” comp. 1 showed a medium probability of adverse hepatic effects (H-HT of 0.65).

Skin sensitivity predictions varied among families. The “Tolans” and “Phenyl benzoate derivatives” families exhibited the highest irritancy, though tapinarof value is also concerning at first glance.

While we acknowledge that most of the pharmacokinetic parameters reported are primarily used for systemic drug development, we believe that their inclusion is valuable. In vivo biological testing will be essential to complement our computational analysis and ensure a thorough safety profile for these compounds.

Discussion

In this study, we employed a multistage computational drug-discovery pipeline to explore the chemical space around tapinarof, a known AhR agonist approved for psoriasis treatment. Our docking results on the tapinarof molecule align with the recent experimental data and provide a solid foundation for identifying other compounds capable of activating AhR. By conducting a 3D similarity search in PubChem, we identified 305 compounds, among which we found interesting families. However, these compounds were structurally too similar to tapinarof and were already described in the tapinarof patents. Further expanding the search, we screened 19,943 additional compounds and identified four major promising families with favorable docking scores: “Tolans”, “Alkene-to-three-membered-ring cyclization”, “Phenyl benzoate derivatives”, and “Alkene-to-imes/azo” compounds. Molecular dynamics simulations on the docking poses of the most promising compounds confirmed the stability of most of them, evidencing only a few that may result in reduced affinity compared to the docking predictions. The diverse scaffolds identified in this expanded search suggested that non-traditional structural motifs, beyond tapinarof analogues, may offer new therapeutic opportunities for psoriasis and other AhR-related diseases.

Interestingly, we found data supporting further investigation into certain families of compounds. Tolans, for example, are a class of compounds already patented for their use as cosmetics or therapeutics for skin conditions⁵⁴. Surprisingly, we discovered that the patent is related to the use of tolans as modulators of sirtuin activity. Sirtuins are a family of enzymes, named after the yeast protein Sir2, which play a crucial role in regulating cellular processes such as aging, stress responses, and metabolism⁵⁵. AhR and sirtuins, particularly SIRT1 and SIRT3, exhibit a bidirectional regulatory relationship with implications for skin health and inflammation⁵⁶. AhR activation suppresses SIRT1 by reducing NAD⁺ levels, accelerating senescence⁵⁷, while SIRT1 enhances AhR-driven processes, including filaggrin expression⁵⁸. SIRT1 depletion in keratinocytes has been reported to inhibit both basal and ligand-induced AhR activation, while its presence enhances AhR-driven processes, including AhR/AKT-induced filaggrin expression, which is crucial for skin barrier function⁵⁹. Moreover, AhR activation inhibits SIRT3 via TiPARP-induced NAD⁺ depletion, increasing oxidative stress through SOD2 acetylation⁶⁰. The identification of tolans as AhR modulators suggests they might influence both sirtuins and AhR signaling, key players in psoriasis pathogenesis. Interestingly, tapinarof itself shares structural similarity with resveratrol, piceatannol, and other known sirtuin activators. This raises the possibility that its therapeutic effects may extend beyond AhR activation to include sirtuin modulation. Supporting this, in the work of Smith et al.⁴³ the molecular profiling experiment showed that tapinarof moderately activates SIRT1, while resveratrol—a well-established SIRT1 activator—was less potent in the same assay. Given the established crosstalk between AhR and sirtuins, further investigation is warranted to determine whether sirtuin activation contributes to tapinarof efficacy in psoriasis, potentially offering a dual mechanism of action that enhances skin barrier integrity and mitigates inflammation. This dual regulation opens new therapeutic perspectives, where targeting both pathways could help manage inflammation, oxidative stress, and skin barrier function.

Other compounds also emerged as particularly noteworthy. One member of the “alkene to three-membered ring cyclization” family, Gnetumelin C (Supplementary Fig. 11a), is a naturally occurring compound known for its anti-inflammatory, antimicrobial, and antioxidant properties. It has been proposed as a promising ingredient

in cosmetic formulations aimed at skin protection and anti-aging applications⁶¹. The top-performing compound within the “phenyl benzoate derivatives” (Fig. 5) shares structural similarity with ellagic acid, a naturally occurring hetero-tetracyclic compound found in various fruits and vegetables. Ellagic acid exhibits antioxidant and anti-proliferative effects and has been studied for the topical treatment of melasma⁶². Additionally, other molecules within the “phenyl benzoate derivatives” class are particularly interesting, as their unsaturated lactone core represents the structural backbone of coumarin derivatives. These compounds are studied in inflammatory bowel diseases for their ability to activate the AhR/Nrf2 pathways^{63,64}.

To further refine the search for effective AhR modulators, a pharmacophore model using SAR analysis could be developed based on the key interactions observed in our dataset. This approach would identify essential pharmacophoric features required for AhR binding, facilitating the rational design of novel analogs with improved affinity. Such a model could also be verified on a set of known AhR ligands and employed in virtual screening campaigns to identify additional promising candidates beyond the chemical space explored in this study.

Overall, our findings underscore the potential of computational drug-discovery in identifying novel AhR modulators, broadening the spectrum of candidates for experimental validation. Indeed, while computational approaches provide valuable insights, experimental validation remains crucial to confirm the interactions of these compounds with AhR and assess their biological activity. Future studies should focus on experimental assays to evaluate the therapeutic potential of these compounds in psoriasis and other AhR-related diseases. Notably, starting from the tapinarof chemical scaffold, our approach identified molecules with potential involvement in other psoriasis-related pathways, as well as compounds structurally similar to established AhR ligands. This adds further value to our findings, suggesting that these compounds are worthy of further experimental investigation in future studies.

Methods

PubChem search

To identify novel AhR modulators, we employed a systematic multi-stage ligand search strategy using the PubChem database⁶⁵. PubChem provides several tools for ligand-based searching, including 2D similarity, 3D similarity, and substructure searches. The multi-stage search strategy is outlined in Supplementary Fig. 3 and Supplementary Fig. 8.

The 2D similarity search in PubChem relies on molecular fingerprints, which encode the presence or absence of specific substructural patterns within a molecule. The search algorithm computes a similarity score, typically using the Tanimoto coefficient, to compare the query molecule with the compounds in the database. This approach enables the retrieval of structurally-related compounds that share common functional groups and topological features with the query molecule. For our study, we used the PubChem 2D similarity search tool in the second step of the multi-stage search strategy, querying against tapinarof, with the default Tanimoto threshold of 0.9.

Unlike 2D searches, which rely on molecular connectivity, 3D similarity searches evaluate the spatial conformation of molecules. PubChem 3D search algorithm compares the three-dimensional shape and electrostatic properties of a query molecule against the conformers stored in its database. The scoring function ranks molecules based on shape similarity and pharmacophoric match, providing a set of molecules that may preserve binding modes of the reference ligand. For our study, we used the PubChem 3D similarity search tool in both the first and second steps of the multi-stage search strategy. In the first step, we queried against tapinarof analogs, and in the second step, we expanded the search by querying against 1,3-dichloro-5-(2-phenylethenyl) benzene. The choice of chlorinated trans-stilbene as the target for the 3D similarity search was made because, despite non-hydroxylated trans-stilbenes are known to be good binders of AhR, they were not retrieved in the first 3D similarity search against tapinarof, which predominantly returned molecules with one or more hydrogen donor groups.

The substructure search tool in PubChem identifies compounds containing a specific molecular core scaffold. This approach is useful for exploring chemical families that share the desired scaffold with the reference compound while allowing for significant variations in the functional groups. To expand our search space, we used the substructure search based on key scaffolds identified in the second step of the multi-stage search. Given that the substructure search may return molecules that differ significantly from the original compound, as long as they contain the searched substructure, we applied filters on size (molecular weight < 300 g/mol) and hydrophobicity ($-1 < \log P < 5$) to reduce the number of compounds obtained from the search, while remaining close to the queried ligand. The filter on hydrophobicity was not applied to the family of compounds with three-membered ring substitution of the central double bond, as the number of compounds retrieved for this family was already small.

Molecular docking

The structure of the human AhR PAS-B domain (PDB ID: 7ZUB)¹⁹ was obtained from the Protein Data Bank. This cryo-EM structure includes the AhR PAS-B domain complexed with the indirubin ligand and the hsp90 and XAP2 proteins that constitute its cytosolic assembly. For docking calculations, non-AhR proteins were removed, and the resulting structure was preprocessed using Schrödinger's Protein Preparation Wizard⁶⁶. Residue protonation states were assigned with PROPKA⁶⁷ at pH 7.0.

The structures of the ligands were downloaded from PubChem in the sdf format and then prepared with the LigPrep utility in the Schrödinger 2024-2 suite⁶⁸. Their protonation states were determined with the Epik Classic tool for pKa prediction included in Maestro⁶⁹, which is based on PROPKA as a heuristic pKa calculator.

Docking was performed using Glide XP⁷⁰ (extra precision). This method uses a hierarchical series of filters to search for possible locations of the ligand in the binding site and includes a flexible treatment of the ligand. The

shape and properties of the protein are represented on a grid by different sets of fields that provide progressively more accurate scoring of the ligand poses. Glide XP performs extensive sampling for ligand positioning through an anchor-and-grow approach and also accounts for explicit waters. The method uses a scoring function (XP GlideScore) that includes force-field-based functions to describe Coulomb and van der Waals contributions to the interaction energy as well as empirically based functions. The receptor grid for the AhR PAS-B domain was centered on the center of mass of the indirubin ligand in the experimental structure. Docking calculations employed the following parameters: (a) Retain up to 50,000 poses per ligand during the initial docking phase. (b) Use a scoring window of 200 kcal/mol to select initial poses. (c) Retain up to 2,000 poses per ligand for energy minimization. (d) Apply expanded sampling to increase thoroughness.

Ligands cluster analysis

To analyze the results of the virtual screening for the large dataset of ligands obtained in stage 2, we performed a cluster analysis of the ligands that displayed a docking score lower than -9.5 kcal/mol. This threshold was chosen to include only ligands with docking scores within 1 kcal/mol of the score obtained for tapinarof. The subset of ligands meeting this criterion was clustered using the Canvas Similarity and Clustering tool in Maestro. We used a linear fingerprint type with the atom typing scheme 12 (Daylight invariant atom types, where bonds are distinguished by bond order, and cyclic aliphatic structures are distinguished from acyclic aliphatic ones). Similarity was computed using the Tanimoto similarity metric, and results were then clustered using the complete linkage method. The optimal number of clusters was determined based on the Kelley Penalty score. Clusters were analyzed to identify families of ligands that displayed consistently favorable docking scores.

Molecular dynamics

The complexes of tapinarof and the most promising compounds from each chemical family, identified through molecular docking, were subjected to molecular dynamics (MD) simulations. Each system was prepared using the tleap module of the AMBER19⁷¹ package, employing the ff19SB⁷² force field for the protein. Solvation was performed with OPC water molecules⁷³, extending up to 12 Å from the solute, and neutralization was achieved with Na⁺/Cl⁻ ions. An additional excess of ions was added to reach a final salt concentration of 0.15 M. Ligand parametrization was conducted using the antechamber module and the Generalized Amber Force Field (GAFF2)⁷⁴. Atomic partial charges were assigned using the RESP fitting procedure after HF/6-31G* geometry optimization in vacuum and electrostatic potential calculations with Gaussian16⁷⁵.

To ensure a stable and physically meaningful starting conformation, a multi-stage equilibration protocol was applied⁷⁶. Initially, steepest descent and conjugate gradient energy minimization were performed in two steps: (i) restraining the solute to relax the solvent molecules, followed by (ii) unrestrained minimization of the entire system. The system was then gradually heated to 300 K over 2 ns under the NVT ensemble, with harmonic restraints ($100 \text{ kcal}\cdot\text{mol}^{-1}\cdot\text{Å}^{-2}$) applied to the solute during heating. Subsequently, equilibration under NPT conditions was conducted in two consecutive 1 ns runs, during which the restraints were gradually reduced from $100 \text{ kcal}\cdot\text{mol}^{-1}\cdot\text{Å}^{-2}$ to $10 \text{ kcal}\cdot\text{mol}^{-1}\cdot\text{Å}^{-2}$. The Berendsen⁷⁷ barostat was used to maintain a pressure of 1 atm with a relaxation time of 1 ps. A second minimization step was then performed, removing the restraints on protein side chains. Further equilibration consisted of three additional 1 ns NPT runs, during which the restraints were progressively decreased ($10 \text{ kcal}\cdot\text{mol}^{-1}\cdot\text{Å}^{-2}$, $1 \text{ kcal}\cdot\text{mol}^{-1}\cdot\text{Å}^{-2}$, and $0.1 \text{ kcal}\cdot\text{mol}^{-1}\cdot\text{Å}^{-2}$ on backbone and ligand heavy atoms). A final unrestrained NPT equilibration of 1 ns was performed to achieve proper density and system stabilization before production runs. A time step of 1.0 fs was used during all equilibration stages, while a time step of 2.0 fs was employed for the subsequent 3×100 ns production runs, using the SHAKE algorithm to constrain bonds involving hydrogen atoms.

The binding free energy for complex formation was evaluated using the Molecular Mechanics Generalized Born Surface Area (MM-GBSA) method^{78,79} implemented in AMBER, which employs an implicit solvent model⁸⁰. The single-trajectory approach was selected, meaning that the conformational ensemble was extracted from the single trajectory of the complex rather than from the separate trajectories of the complex, receptor, and ligand. An ensemble of 900 conformations, regularly sampled from the equilibrated portion of the production run (10–100 ns), was used for ΔG_{bind} calculations.

Pharmacokinetics and toxicity analysis

Pharmacokinetics analyzes the body's response to the drugs and the way in which the body affects the drugs being administered. This analysis is based on four different factors, which include absorption, distribution, metabolism, and excretion of drugs⁸¹. A series of physico-chemical and biological properties were predicted using the ADMETlab 2.0 server⁴⁹. Moreover, the Skin Permeation parameter ($\log K_p$) was predicted using SwissADME⁵⁰. The structures of the four most promising compounds of each chemical family, and tapinarof, were analyzed using these tools. The SMILES files of the targeted ligands were given as input to the servers to predict key ADMET parameters. Based on the results produced, it was inferred whether the targeted ligands/compounds would possess the characteristics for pharmacological formulation.

Data availability

The datasets generated during and/or analyzed during the current study are available from the corresponding author on reasonable request.

Received: 19 February 2025; Accepted: 21 May 2025

Published online: 06 June 2025

References

- Larigot, L., Juricek, L., Dairou, J. & Coumoul, X. AhR signaling pathways and regulatory functions. *Biochim. Open* **7**, 1–9 (2018).
- Esser, C. & Rannug, A. The Aryl hydrocarbon receptor in barrier organ physiology, immunology, and toxicology. *Pharmacol. Rev.* **67**, 259–279 (2015).
- Murray, I. A. & Perdew, G. H. How ah receptor ligand specificity became important in Understanding its physiological function. *Int. J. Mol. Sci.* **21**, 9614 (2020).
- Wright, E. J., De Castro, P., Joshi, K., Elferink, C. J. & A. D. & Canonical and non-canonical Aryl hydrocarbon receptor signaling pathways. *Curr. Opin. Toxicol.* **2**, 87–92 (2017).
- Riaz, F., Pan, F. & Wei, P. Aryl hydrocarbon receptor: the master regulator of immune responses in allergic diseases. *Front Immunol* **13**, (2022).
- Sondermann, N. C. et al. Functions of the Aryl hydrocarbon receptor (AHR) beyond the canonical AHR/ARNT signaling pathway. *Biochem. Pharmacol.* **208**, 115371 (2023).
- Stockinger, B., Di Meglio, P., Gialitakis, M. & Duarte, J. H. The Aryl hydrocarbon receptor: multitasking in the immune system. *Annu. Rev. Immunol.* **32**, 403–432 (2014).
- Rothhammer, V. & Quintana, F. J. The Aryl hydrocarbon receptor: an environmental sensor integrating immune responses in health and disease. *Nat. Rev. Immunol.* **19**, 184–197 (2019).
- Poland, A. & Knutson, J. C. 2,3,7,8-Tetrachlorodibenzo-p-Dioxin and related halogenated aromatic hydrocarbons: examination of the mechanism of toxicity. *Annu. Rev. Pharmacol. Toxicol.* **22**, 517–554 (1982).
- Lin, L., Dai, Y. & Xia, Y. An overview of Aryl hydrocarbon receptor ligands in the last two decades (2002–2022): A medicinal chemistry perspective. *Eur. J. Med. Chem.* **244**, 114845 (2022).
- Denison, M. S., Soshilov, A. A., He, G., DeGroot, D. E. & Zhao, B. Exactly the same but different: promiscuity and diversity in the molecular mechanisms of action of the Aryl hydrocarbon receptor (dioxin) receptor. *Toxicol. Sci.* **124**, 1–22 (2011).
- DeGroot, D. et al. AHR Ligands: Promiscuity in Binding and Diversity in Response. in *The AH Receptor in Biology and Toxicology* (ed. Pohianvirta R) 63–79 (John Wiley & Sons, (2011).
- Veldhoen, M. et al. The Aryl hydrocarbon receptor links TH17-cell-mediated autoimmunity to environmental toxins. *Nature* **453**, 106–109 (2008).
- Quintana, F. J. et al. Control of Treg and TH17 cell differentiation by the Aryl hydrocarbon receptor. *Nature* **453**, 65–71 (2008).
- Dvořák, Z., Sokol, H. & Mani, S. Drug mimicry: promiscuous receptors PXR and AhR, and microbial metabolite interactions in the intestine. *Trends Pharmacol. Sci.* **41**, 900–908 (2020).
- Denison, M. S. & Faber, S. C. And now for something completely different: diversity in ligand-dependent activation of ah receptor responses. *Curr. Opin. Toxicol.* **2**, 124–131 (2017).
- Soshilov, A. A., Motta, S., Bonati, L. & Denison, M. S. Transitional States in ligand-dependent transformation of the Aryl hydrocarbon receptor into its DNA-binding form. *Int. J. Mol. Sci.* **21**, 3–6 (2020).
- Bonati, L., Motta, S. & Callea, L. The AhR signaling mechanism: A structural point of view. *J. Mol. Biol.* **436**, 168296 (2024).
- Gruszczak, J. et al. Cryo-EM structure of the agonist-bound Hsp90-XAP2-AHR cytosolic complex. *Nat. Commun.* **13**, 7010 (2022).
- Motto, I., Bordogna, A., Soshilov, A. A., Denison, M. S. & Bonati, L. New Aryl hydrocarbon receptor homology model targeted to improve Docking reliability. *J. Chem. Inf. Model.* **51**, 2868–2881 (2011).
- Giani Tagliabue, S., Faber, S. C., Motta, S., Denison, M. S. & Bonati, L. Modeling the binding of diverse ligands within the ah receptor ligand binding domain. *Sci Rep* **9**, (2019).
- Corrada, D., Denison, M. S. & Bonati, L. Structural modeling of the AhR:ARNT complex in the bHLH-PASA-PASB region elucidates the key determinants of dimerization. *Mol. Biosyst.* **13**, 981–990 (2017).
- Pandini, A., Denison, M. S., Song, Y., Soshilov, A. A. & Bonati, L. Structural and functional characterization of the Aryl hydrocarbon receptor ligand binding domain by homology modeling and mutational analysis. *Biochemistry* **46**, 696–708 (2007).
- Motta, S. & Bonati, L. TCDD-Induced allosteric perturbation of the AhR:ARNT binding to DNA. *Int. J. Mol. Sci.* **24**, 9339 (2023).
- Kwong, H. S. et al. Structural insights into the activation of human Aryl hydrocarbon receptor by the environmental contaminant Benzo[a]pyrene and structurally related compounds. *J. Mol. Biol.* **436**, (2024).
- Wen, Z. et al. Cryo-EM structure of the cytosolic AhR complex. *Structure* **31**, 295–308e4 (2023).
- Diao, X. et al. Structural basis for the ligand-dependent activation of heterodimeric AHR-ARNT complex. *Nat. Commun.* **16**, 1282 (2025).
- Keam, S. J. Tapinarof cream 1%: first approval. *Drugs* **82**, 1221–1228 (2022).
- Rangarajan, P., Karthikeyan, A. & Dheen, S. T. Role of dietary phenols in mitigating microglia-mediated neuroinflammation. *Neuromolecular Med.* **18**, 453–464 (2016).
- De Leo, A., Arena, G., Stecca, C., Raciti, M. & Mattia, E. Resveratrol inhibits proliferation and survival of epstein barr Virus-Infected Burkitt's lymphoma cells depending on viral latency program. *Mol. Cancer Res.* **9**, 1346–1355 (2011).
- Chimento, A. et al. Resveratrol and its analogs as antitumoral agents for breast Cancer treatment. *Mini-Reviews Med. Chem.* **16**, 699–709 (2016).
- Kubota, S. et al. Prevention of ocular inflammation in Endotoxin-Induced uveitis with Resveratrol by inhibiting oxidative damage and nuclear Factor- κ B activation. *Invest. Ophthalmology Visual Sci.* **50**, 3512 (2009).
- Howitz, K. T. et al. Small molecule activators of sirtuins extend *Saccharomyces cerevisiae* lifespan. *Nature* **425**, 191–196 (2003).
- Mohammadi-Bardbori, A. et al. Resveratrol, and Curcumin are indirect activators of the Aryl hydrocarbon receptor (AHR). *Chem. Res. Toxicol.* **25**, 1878–1884 (2012).
- Gouédard, C., Barouki, R. & Morel, Y. Induction of the Paraoxonase-1 gene expression by Resveratrol. *Arterioscler. Thromb. Vasc. Biol.* **24**, 2378–2383 (2004).
- Lee, J. E. & Safe, S. Involvement of a post-transcriptional mechanism in the Inhibition of CYP1A1 expression by Resveratrol in breast cancer cells. *Biochem. Pharmacol.* **62**, 1113–1124 (2001).
- Casper, R. F. et al. Resveratrol has antagonist activity on the Aryl hydrocarbon receptor: implications for prevention of Dioxin toxicity. *Mol. Pharmacol.* **56**, 784–790 (1999).
- Ciolino, H. P., Daschner, P. J. & Yeh, G. C. Resveratrol inhibits transcription of CYP1A1 in vitro by preventing activation of the Aryl hydrocarbon receptor. *Cancer Res.* **58**, 5707–5712 (1998).
- Pastorková, B., Vrzalová, A., Bachleda, P. & Dvořák, Z. Hydroxystilbenes and methoxystilbenes activate human Aryl hydrocarbon receptor and induce CYP1A genes in human hepatoma cells and human hepatocytes. *Food Chem. Toxicol.* **103**, 122–132 (2017).
- Bissonnette, R. et al. Efficacy and safety of topical WBI-1001 in patients with mild to severe atopic dermatitis: results from a 12-week, multicentre, randomized, placebo-controlled double-blind trial. *Br. J. Dermatol.* **166**, 853–860 (2012).
- Bissonnette, R. et al. Efficacy and safety of topical WBI-1001 in patients with mild to moderate psoriasis: results from a randomized double-blind placebo-controlled, phase II trial. *J. Eur. Acad. Dermatol. Venereol.* **26**, 1516–1521 (2012).
- Bissonnette, R. et al. Efficacy and safety of topical WBI-1001 in the treatment of atopic dermatitis: results from a phase 2A, randomized, Placebo-Controlled clinical trial. *Arch Dermatol* **146**, (2010).
- Smith, S. H. et al. Tapinarof is a natural AhR agonist that resolves skin inflammation in mice and humans. *J. Invest. Dermatology.* **137**, 2110–2119 (2017).

44. Bissonnette, R., Stein Gold, L., Rubenstein, D. S., Tallman, A. M. & Armstrong A. Tapinarof in the treatment of psoriasis: A review of the unique mechanism of action of a novel therapeutic Aryl hydrocarbon receptor–modulating agent. *J. Am. Acad. Dermatol.* **84**, 1059–1067 (2021).
45. Furue, M. et al. Antioxidants for Healthy Skin: The Emerging Role of Aryl Hydrocarbon Receptors and Nuclear Factor-Erythroid 2-Related Factor-2. *Nutrients* **9**, 223 (2017).
46. Haarmann-Stemmann, T., Sutter, T. R., Krutmann, J. & Esser, C. The mode of action of Tapinarof May not only depend on the activation of cutaneous Aryl hydrocarbon receptor signaling but also on its antimicrobial activity. *J. Am. Acad. Dermatol.* **85**, e33–e34 (2021).
47. Xie, X. et al. Indirubin ameliorates imiquimod-induced psoriasis-like skin lesions in mice by inhibiting inflammatory responses mediated by IL-17A-producing T_H17 cells. *Mol. Immunol.* **101**, 386–395 (2018).
48. Basciu, A. et al. No dance, no partner! A Tale of receptor flexibility in Docking and virtual screening. *Annu. Rep. Med. Chem.* **59**, 43–97 (2022).
49. Xiong, G. et al. ADMETlab 2.0: an integrated online platform for accurate and comprehensive predictions of ADMET properties. *Nucleic Acids Res.* **49**, W5–W14 (2021).
50. Daina, A., Michielin, O. & Zoete, V. SwissADME: a free web tool to evaluate pharmacokinetics, drug-likeness and medicinal chemistry friendliness of small molecules. *Sci. Rep.* **7**, 42717 (2017).
51. Lipinski, C. A., Lombardo, F., Dominy, B. W. & Feeney, P. J. Experimental and computational approaches to estimate solubility and permeability in drug discovery and development settings. *Adv. Drug Deliv. Rev.* **23**, 3–25 (1997).
52. Gleeson, M. P. Generation of a set of simple, interpretable ADMET rules of thumb. *J. Med. Chem.* **51**, 817–834 (2008).
53. Johnson, T. W., Dress, K. R. & Edwards, M. Using the golden triangle to optimize clearance and oral absorption. *Bioorg. Med. Chem. Lett.* **19**, 5560–5564 (2009).
54. Tsai, C. C. Hydroxylated tolans and related compounds as cosmetics or therapeutics for skin conditions. (2009).
55. Preyat, N. & Leo, O. Sirtuin deacylases: a molecular link between metabolism and immunity. *J. Leukoc. Biol.* **93**, 669–680 (2013).
56. Mulero-Navarro, S. & Fernandez-Salguero, P. M. New trends in Aryl hydrocarbon receptor biology. *Front Cell. Dev. Biol.* **4**, (2016).
57. Koizumi, M. et al. Aryl hydrocarbon receptor mediates indoxyl Sulfate-Induced cellular senescence in human umbilical vein endothelial cells. *J. Atheroscler. Thromb.* **21**, 904–916 (2014).
58. van den Bogaard, E. H. et al. Genetic and Pharmacological analysis identifies a physiological role for the AHR in epidermal differentiation. *J. Invest. Dermatol.* **135**, 1320–1328 (2015).
59. Ming, M. et al. Loss of Sirtuin 1 (SIRT1) disrupts skin barrier integrity and sensitizes mice to epicutaneous allergen challenge. *J. Allergy Clin. Immunol.* **135**, 936–945e4 (2015).
60. He, J. et al. Activation of the Aryl hydrocarbon receptor sensitizes mice to nonalcoholic steatohepatitis by deactivating mitochondrial Sirtuin deacetylase Sirt3. *Mol. Cell. Biol.* **33**, 2047–2055 (2013).
61. Gnetumelin, C. <https://www.smolecule.com/products/s13573037>
62. Sivamani, R. & Clark, A. Phytochemicals in the treatment of hyperpigmentation. *Botanics Volume*. **6**, 89–96 (2016).
63. Singh, R. et al. Enhancement of the gut barrier integrity by a microbial metabolite through the Nrf2 pathway. *Nat. Commun.* **10**, 89 (2019).
64. Di Stasi, L. C. Natural coumarin derivatives activating Nrf2 signaling pathway as lead compounds for the design and synthesis of intestinal Anti-Inflammatory drugs. *Pharmaceuticals* **16**, 511 (2023).
65. Kim, S. et al. PubChem 2025 update. *Nucleic Acids Res.* **53**, D1516–D1525 (2025).
66. Madhavi Sastry, G. et al. Protein and ligand preparation: parameters, protocols, and influence on virtual screening enrichments. *J. Comput. Aid Mol. Des.* **27**, 221–234 (2013).
67. Søndergaard, C. R., Olsson, M. H. M., Rostkowski, M. & Jensen, J. H. Improved treatment of ligands and coupling effects in empirical calculation and rationalization of P Ka values. *J. Chem. Theory Comput.* **7**, 2284–2295 (2011).
68. Greenwood, J. R., Calkins, D., Sullivan, A. P. & Shelley, J. C. Towards the comprehensive, rapid, and accurate prediction of the favorable tautomeric states of drug-like molecules in aqueous solution. *Journal of Computer-Aided Molecular Design* vol. 24 591–604 Preprint at (2010). <https://doi.org/10.1007/s10822-010-9349-1>
69. Shelley, J. C. et al. Epik: A software program for pKa prediction and protonation state generation for drug-like molecules. *J. Comput. Aided Mol. Des.* **21**, 681–691 (2007).
70. Friesner, R. A. et al. Extra precision glide: Docking and scoring incorporating a model of hydrophobic enclosure for protein-ligand complexes. *J. Med. Chem.* **49**, 6177–6196 (2006).
71. Case, D. et al. The amber biomolecular simulation programs. *J. Comput. Chem.* **26**, 1668–1688 (2005).
72. Tian, C. et al. ff19SB: Amino-Acid-Specific protein backbone parameters trained against quantum mechanics energy surfaces in solution. *J. Chem. Theory Comput.* **16**, 528–552 (2020).
73. Izadi, S., Anandakrishnan, R. & Onufriev, A. V. Building water models: A different approach. *J. Phys. Chem. Lett.* **5**, 3863–3871 (2014).
74. He, X., Man, V. H., Yang, W., Lee, T. S. & Wang, J. A fast and high-quality charge model for the next generation general AMBER force field. *J. Chem. Phys.* **153**, (2020).
75. Frisch, M. J. et al. Gaussian¹⁶ Revision C.01. Preprint at (2016).
76. Motta, S. & Bonati, L. Modeling binding with large conformational changes: key points in Ensemble-Docking approaches. *J. Chem. Inf. Model.* **57**, 1563–1578 (2017).
77. Berendsen, H. J. C., Postma, J. P. M., Van Gunsteren, W. F., Dinola, A. & Haak, J. R. Molecular dynamics with coupling to an external bath. *J. Chem. Phys.* **81**, 3684–3690 (1984).
78. Hou, T., Wang, J., Li, Y. & E. I. Wang, W. Assessing the performance of the molecular Mechanics / Poisson Boltzmann surface area and molecular Mechanics / Generalized born surface area methods. II. The accuracy of ranking poses generated from Docking. *J. Comput. Chem.* **32**, 866–877 (2011).
79. Kollman, P. A. et al. Calculating structures and free energies of complex molecules: combining molecular mechanics and continuum models. *Acc. Chem. Res.* **33**, 889–897 (2000).
80. Onufriev, A., Bashford, D. & Case, D. A. Exploring protein native States and large-scale conformational changes with a modified generalized born model. *Proteins Struct. Funct. Bioinform.* **55**, 383–394 (2004).
81. Li, Y. et al. Current trends in drug metabolism and pharmacokinetics. *Acta Pharm. Sin B.* **9**, 1113–1144 (2019).

Acknowledgements

This research was supported by the National Psoriasis Foundation USA (Discovery Grant - Award ID: 1298983). We acknowledge CINECA for the availability of high-performance computing resources as part of the agreement with the University of Milano-Bicocca.

Author contributions

S.M and L.B. conceived the presented idea, G.S. performed the computations and analyzed the results, S.M supervised the project, L.B. helped supervise the project, G.S. aided in interpreting the results, S.M. drafted the manuscript and designed the figures. All authors discussed the results and reviewed the manuscript.

Declarations

Competing interests

The authors declare no competing interests.

Additional information

Supplementary Information The online version contains supplementary material available at <https://doi.org/10.1038/s41598-025-03626-z>.

Correspondence and requests for materials should be addressed to L.B. or S.M.

Reprints and permissions information is available at www.nature.com/reprints.

Publisher's note Springer Nature remains neutral with regard to jurisdictional claims in published maps and institutional affiliations.

Open Access This article is licensed under a Creative Commons Attribution-NonCommercial-NoDerivatives 4.0 International License, which permits any non-commercial use, sharing, distribution and reproduction in any medium or format, as long as you give appropriate credit to the original author(s) and the source, provide a link to the Creative Commons licence, and indicate if you modified the licensed material. You do not have permission under this licence to share adapted material derived from this article or parts of it. The images or other third party material in this article are included in the article's Creative Commons licence, unless indicated otherwise in a credit line to the material. If material is not included in the article's Creative Commons licence and your intended use is not permitted by statutory regulation or exceeds the permitted use, you will need to obtain permission directly from the copyright holder. To view a copy of this licence, visit <http://creativecommons.org/licenses/by-nc-nd/4.0/>.

© The Author(s) 2025